E. Manfredi and E. Vitale**

Multiaxial High Temperature Low Cycle Fatigue in AISI 316 Welded Structural Members, and Life Predictions

REFERENCE Manfredi, E. and Vitale, E., **Multiaxial high temperature low cycle fatigue in AISI 316 welded structural members, and life predictions,** *Biaxial and Multiaxial Fatigue*, EGF 3 (Edited by M. W. Brown and K. J. Miller), 1989, Mechanical Engineering Publications, London, pp. 71–85.

ABSTRACT This paper presents the results of experimental work performed on structural welded members of AISI 316 subjected to axial and torsional in-phase low cycle fatigue at 550°C in air.

Tests with different multiaxiality ratios are performed up to rupture, while keeping the nominal equivalent strain range almost constant for all of them.

The results of these tests are illustrated and a complete inelastic analysis of the structural members is presented. Both the geometrical and the metallurgical notch effects are considered in order to evaluate the localized strain peaks near the weld toe.

Finally, life predictions according to several design methods are compared with experimental results.

Introduction

In real structures, phenomena of multiaxial fatigue (1)(2) may influence the strength of weldments. In this case the crack nucleation depends greatly on the notch effects induced by the shape of the weld and by the geometry of the joined parts. The different metallurgical structures of the base material, heat affected zone, and fusion zone also cause plastic strain concentration effects, owing to their differing strain hardening properties.

The influence of a geometrical notch may vary for differing multiaxiality ratios, because it is sensitive to the relative orientation between the imposed loads and the notch itself. The metallurgical notch effect, due to the different cyclic behaviour of the various zones, may be relatively unimportant in high cycle fatigue at ambient temperature, since the elastic properties are quite uniform throughout the joint, while it has a significant impact on the low cycle fatigue resistance, particularly when at high temperatures.

The present work investigated low cycle fatigue resistance in welded tubular model structures of AISI 316 subjected to axial and torsional in-phase strain cycling at 550°C. This behaviour is of interest for the design of the piping systems of liquid metal fast breeder reactors (LMFBRs) and for similar high temperature applications.

* Dipartimento di Costruzioni Meccaniche e Nucleari, University of Pisa, Italy.

Notation

ε_a	Total axial strain
ε_n	Axial strain on the maximum shear stress plane (MSSP)
γ	Total torsional shear strain
γ_m	Shear strain on the MSSP
ε_{eq}	Equivalent, von Mises strain
E	Young modulus
k	Ramberg–Osgood strain-hardening parameter
K_t	Theoretical stress concentration factor
R	Strain rate (multiaxiality) ratio: $\frac{\Delta\gamma}{\Delta\varepsilon_a}$
N_f	Cycles to fatigue failure
n	Ramberg–Osgood strain-hardening exponent

Specimens and materials

Specimen design

The multiaxial experiments were performed on tubular welded structures about 700 mm long (Fig. 1(a)) which were manufactured by joining two 2 in. schedule 40 pipes by means of inert gas tungsten arc welding (GTAW or TIG).

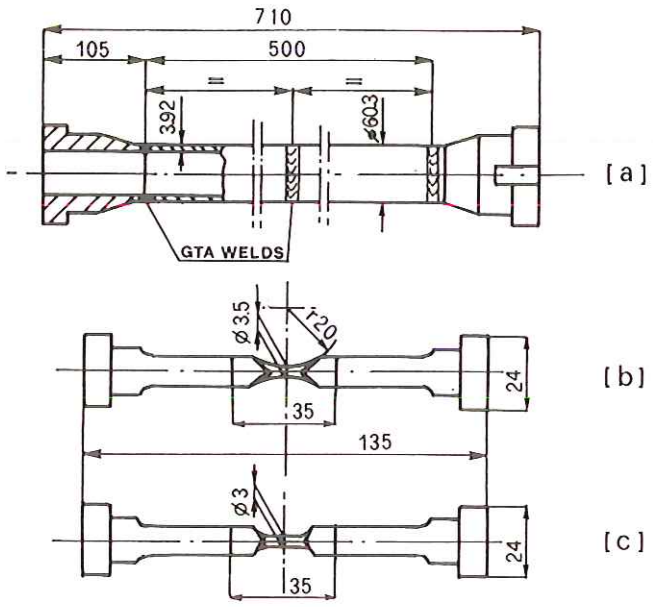

Fig 1 Specimens for (a) multiaxial tests, and (b) and (c) uniaxial tests

Two other GTAW weldments join the tubular part to the flanged ends, which are provided with slotted keyways for the application of torsional loadings.

The design of these specimens was checked for conformity with ASME III B&PV Code Case N47 (**3**) rules, to obtain similarity with a Class 1 nuclear component and to satisfy requirements for avoiding ratchetting, buckling, and creep instability problems. The GTAW weldments were designed, manufactured, and subjected to radiographic controls in accordance with ASME III Class B joint requirements.

Cyclic strain hardening properties and uniaxial low cycle fatigue resistance were evaluated by uniaxial testing on smooth specimens. The specimens were manufactured by lathe turning, grinding, and final polishing from the thin gauge (3.9 mm) base material and fusion zone of the tubular specimens.

Both hourglass specimens for fatigue testing, conforming to ASTM E606 standards, and cylindrical ones for the evaluation of cyclic response (**5**) were used (see Figs 1(b) and 1(c)).

Some base material specimens were subjected to a thermal cycle which simulated the effect of the welding process in the heat affected zone (HAZ). In this way the metallurgical structure of the small specimens was modified in such a way as to become similar to that of the HAZs of the multiaxial specimen. Details of this procedure are given in (**4**).

Material

The material used for fabrication of the tubular part of the specimens was an AISI 316 austenitic stainless steel, chemical composition of which is given in Table 1.

The pipes were fabricated for the Italian LMFBR 'PEC', then nearing completion and strict quality assurance requirements were imposed during their manufacture and inspection.

The flanged ends were manufactured from another heat of AISI 316. Since they are less stressed than the tubular part of the specimen their behaviour is relatively unimportant.

Weldments

The GTAW weldments were performed by the pulsed arc technique, without filler metal, under internal and external argon shielding. Welding was done by the C.R.E. 'Casaccia' Laboratories of the ENEA by means of a fully automatic

Table 1 Chemical composition of base and weld materials (vol. %)

	C	*Mn*	*P*	*S*	*Si*	*Ni*	*Cr*	*Mo*	*Co*	*N*	*δ-ferrite*
Base	0.051	1.78	0.018	0.012	0.56	12.82	16.83	2.78	0.05	0.06	–
Weld	0.044	1.75	0.011	0.012	0.57	12.89	16.93	2.43	0.05	0.06	0.3

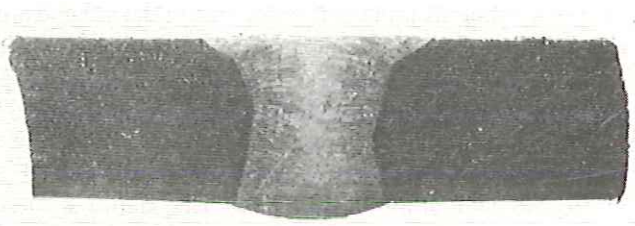

Fig 2 Typical cross-section shape of central welds in multiaxial specimens ('best' shape)

apparatus, the true weld bead shapes varying between slightly differing 'worst' and 'best' ones. A typical weld shape is illustrated in Fig. 2.

Radiographic examination after welding was used to discard defective weldments.

Chemical analyses and delta-ferrite measurements were performed, and their results are given in Table 1. The metallurgical structures of the base material, of the HAZ, and of the fusion zone are illustrated in Fig. 3. The grain size of the base material is about ASTM 7. Typical cold pilgering streaks are visible, especially in the inner part of the tubes. The HAZ is very thin (maximum 1–2 mm) and its structure shows very enlarged grains, varying between ASTM 2 and 5.5.

Experimental apparatus

Smooth specimen testing

A standard 100 kN MTS testing apparatus was used. Special water-cooled grips for the very small gauge specimens (minimum diameter 3.5 mm) were designed for these experiments. The specimens were heated by an electrical muffle furnace.

The uniaxial tests were all performed in strain control with triangular wave shape and a constant strain rate of $1 \cdot 10^{-3}$ (s^{-1}), using a diametral extensometer with quartz rods. Further details are given in (**5**).

Multiaxial testing

A special purpose 300 kN axial testing apparatus, designed and built at the University of Pisa, was modified with the purpose of applying torsional loadings as well as axial ones. The testing apparatus is schematically illustrated in Fig. 4.

The specimens are heated by means of electrical resistance heaters internally mounted. Temperatures up to 700°C are possible. After the heating transient, the temperature at any point of the tubular part falls within ±2 per cent of the nominal value, the variation with time being less than 1 per cent during the tests.

The flanged ends of the specimens are held by water-cooled grips. The lower grip is connected to a 300 kN hydraulic actuator which applies the axial loading.

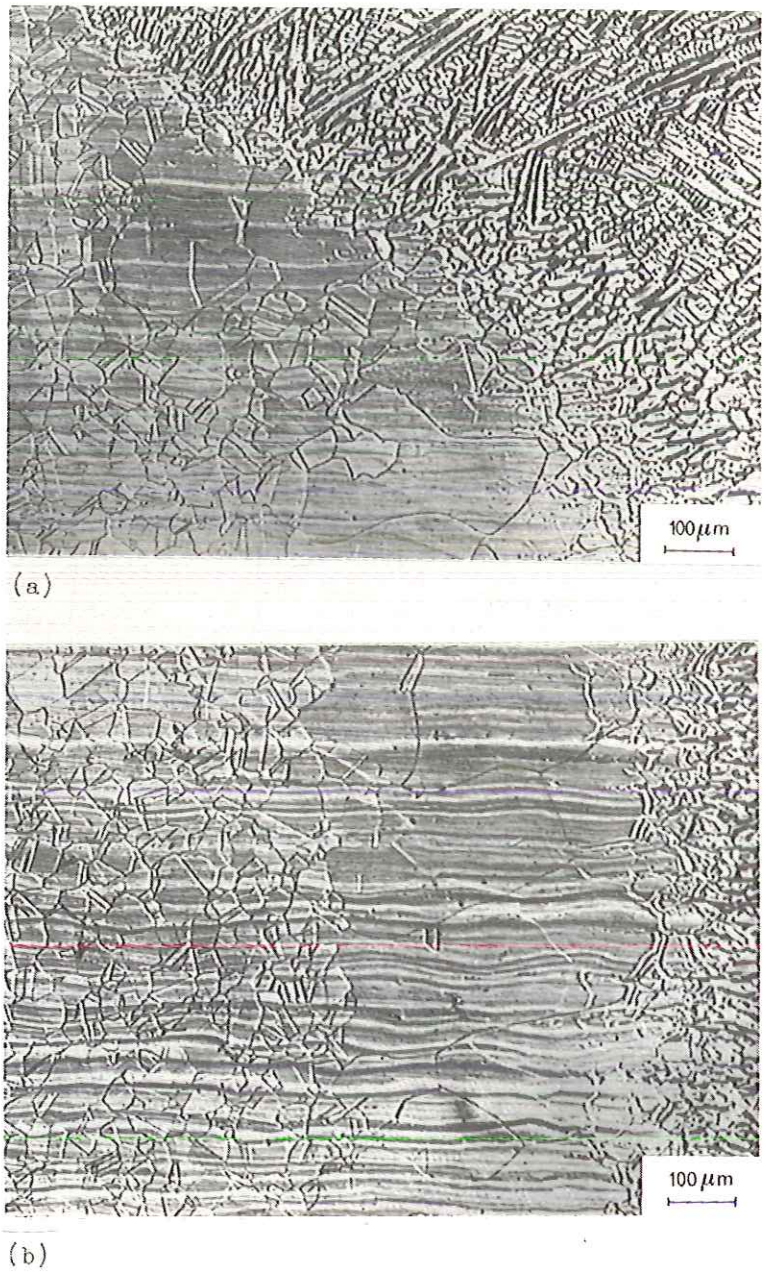

Fig 3 Metallurgical structures. From left to right: base material, HAZ, and fusion zone, (a) near the external surface, and (b) at the mean radius

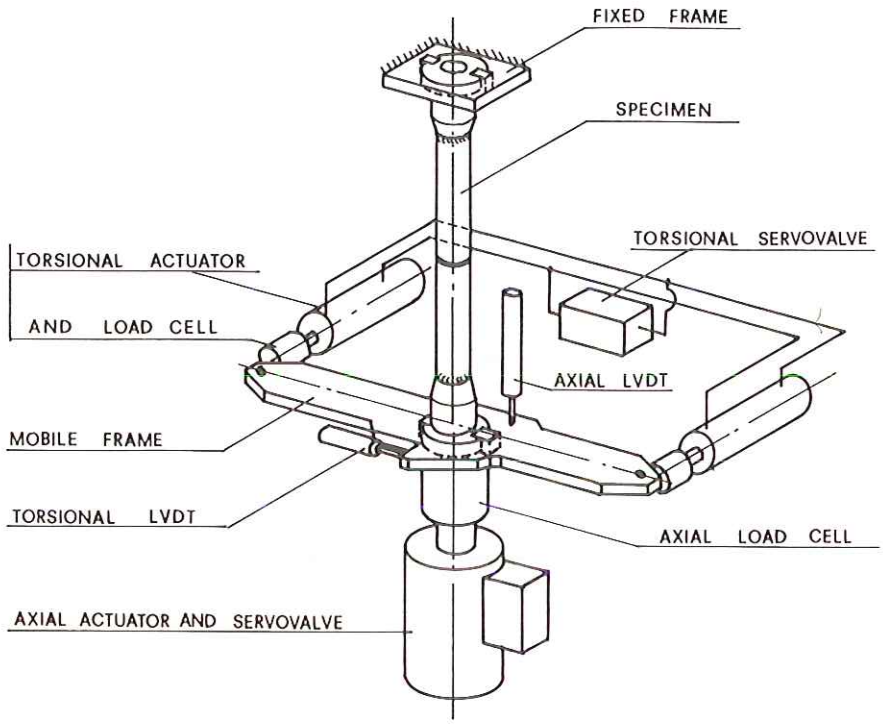

Fig 4 Schematic of multiaxial test equipment

By means of the slotted keyways the flanged ends are connected to torsional holding frames. The lower, mobile, torsional frame is connected to two hydraulic actuators of 4 kN each, which apply up to about 4 kNm of torsional loading.

A standard two-channel MTS servoamplifier operates two servovalves connected to the axial and to the two torsional hydraulic actuators, respectively. Feedback signals are provided by axial and torsional LVDTs and load cells. Loading measurements make use of the single axial load cell and of the average value of the two torsional load cells.

All tests referred to in this work were performed in displacement control, i.e., by controlling the axial and angular displacements of the mobile holding frame. A continuous triangular wave shape was used, corresponding to an equivalent nominal strain rate of $1 \cdot 10^{-3}$ (s^{-1}).

Experimental results

Smooth specimen cyclic stress–strain curves

The evaluation of the cyclic stress–strain behaviour of the various zones of welded structures is of importance for low cycle fatigue resistance prediction,

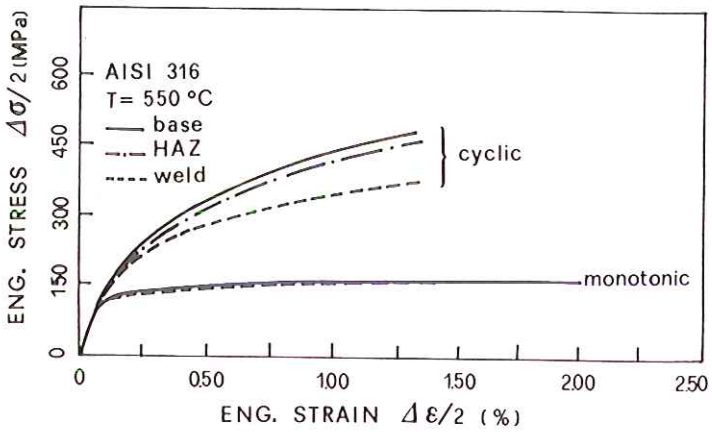

Fig 5 Cyclic and monotonic stress–strain curves for base, HAZ, and weld materials

since it makes it possible to evaluate the strain concentration effects induced by the different cyclic strain hardening properties of base material, HAZ, and fusion zone.

The cyclic properties of the material of these zones at 550°C were measured by means of the multiple-step method (5). Three specimens were used for each zone and the data were reduced by an optimized regression analysis to determine reliable average behaviour for each zone of the material.

The constitutive law used in the analysis was of the Ramberg–Osgood type

$$\Delta\varepsilon/2 = \Delta\sigma/2E + (\Delta\sigma/2k)^{1/n} \quad (1)$$

where E is the elastic modulus and k and n are regression parameters.

Averaged cyclic and monotonic curves are shown in Fig. 5, while optimized parameters for equation (1) are given in Table 2.

It may be observed that the cyclic strain hardening properties of the fusion zone are significantly inferior to those of the HAZ and base material, while the latter two show a very similar cyclic behaviour.

Table 2 Material parameters for equation (1) (cyclic curves)

Material	T (°C)	*Young's modulus (MPa)*	k (*MPa*)	1/n
Base	550	157 200	1869	3.38
Weld	550	152 100	1126	4.14
HAZ	550	157 200	1984	3.20

Low cycle fatigue resistance

The uniaxial low cycle fatigue of the material of the various zones was also checked by continuous cycling strain controlled tests. In this way it was verified that at 550°C the low cycle fatigue resistance of the base material correlates closely with published data (6)(7) for AISI 316. It was also found that the low cycle fatigue resistance of the HAZ and fusion zone does not differ significantly from the resistance of the base material. Hence, a single life relationship, fitted to experimental data from several sources (6) in the range between about 500 and 20 000 cycles, will be used for all the zones of the weld joint

$$\ln (10 \times \Delta\varepsilon_{eq}) = 10.42 \times N_f^{-0.2} \qquad (2)$$

where $\Delta\varepsilon_{eq}$ is the von Mises equivalent strain range (per cent).

Total strain was chosen instead of plastic strain since this latter parameter is not always available from published fatigue results.

In Fig. 6 the fatigue behaviour expressed by this relationship is compared with the fatigue data reported in (6), in terms of maximum plastic shear strain vs. cycles to failure.

Multiaxial tests

Up to now six tests have been performed at 550°C in air. The controlling parameter was the nominal equivalent von Mises strain range, evaluated with reference to a uniform elasto–plastic deformation of the specimen.

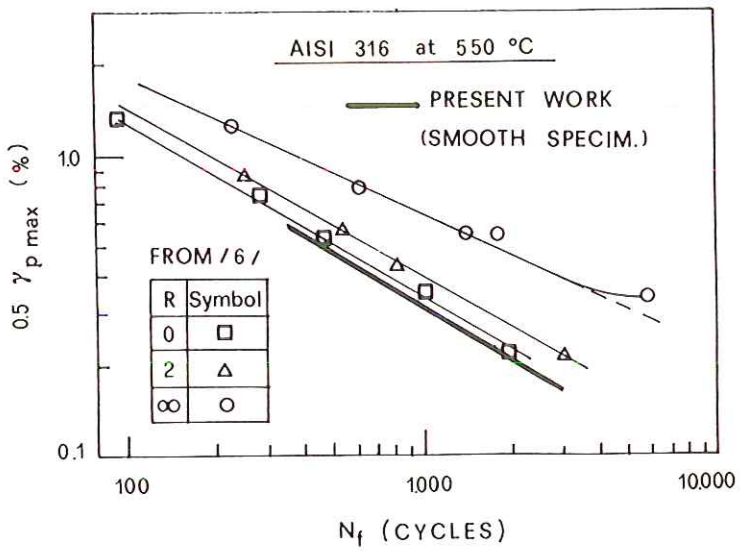

Fig 6 Correlation of smooth-specimen data with results in reference (6), in terms of maximum plastic shear strain

Table 3 Nominal parameters and results of multiaxial specimens testing

Test No.	R	T (°C)	$\dot{\varepsilon}_{eq} \cdot 10^{-3}$ (s^{-1})	$\Delta\varepsilon_a$ (%)	$\Delta\gamma$ (%)	$\Delta\varepsilon_{eq}$ (%)	N_f (*cycles*)	*Rupture position*
108	0	550	0.89	0.640	–	0.596	1424	Weld (C)
102	0	550	0.91	0.510	–	0.478	2695	Weld (C)
104	0	550	0.88	0.361	–	0.335	10 558	Weld (C)
125	1.2	550	0.94	0.483	0.557	0.565	1910	Weld (F)
143	1	550	1.02	0.543	0.550	0.611	1592	Weld (F)
126	3.4	550	1.01	0.260	0.876	0.565	11 085	Tube
145	3.4	550	1.02	0.265	0.887	0.571	6330	Weld (F)
124	∞	550	1.01	–	0.876	0.506	26 177	Tube
144	∞	550	1.00	–	0.728	0.420	19 750	Weld (F)

(C) Central.
(F) Flange.

Three states of strain, corresponding to R values of 1, 3.4, and ∞ were used, performing two tests for each value of R, with roughly the same equivalent strain range (0.5 per cent) and with the same equivalent strain rate ($1 \cdot 10^{-3}$ (s^{-1})).

From previous experimental work on tubular specimens of the same type a larger amount of data, obtained in push–pull, nominally uniaxial cyclic strain, was available (8). Owing to the presence of the weldments and to a Poisson effect, a mild multiaxial state of stress and strain existed in these tests also, so an equivalent von Mises strain range was evaluated for the weld zone.

In Table 3 results of the multiaxial tests are summarized and compared with uniaxial data from three tests.

All tests were interrupted after the observation of a fixed amount of reduction of the load-carrying capability of the specimens. This procedure always corresponded to the presence of large through-thickness cracks, particularly after the tests with greater values of the strain state (multiaxiality) ratio. The rupture event was then associated with the beginning of the decreasing portion of the record of load range versus cycles. A 10 per cent reduction of load carrying capability, with respect to the stabilized value at mid test, was considered sufficient for ending a test. The axial load was always chosen as reference quantity, except for the pure torsion tests.

Typical end-of-test cracks are illustrated in Fig. 7. In axial and low biaxiality ratio tests, the main failures started randomly at a weldment, other cracks having nucleated in the other weldments as well. Failures in the tubular part of the specimen were observed only in pure torsion and high biaxiality ratio tests.

Finite element inelastic analysis

The true cyclic strain pattern which prevailed during the multiaxial fatigue experiments is not known, since it was not feasible to measure experimentally the highly localized strain peaks around the weldments. For this reason an

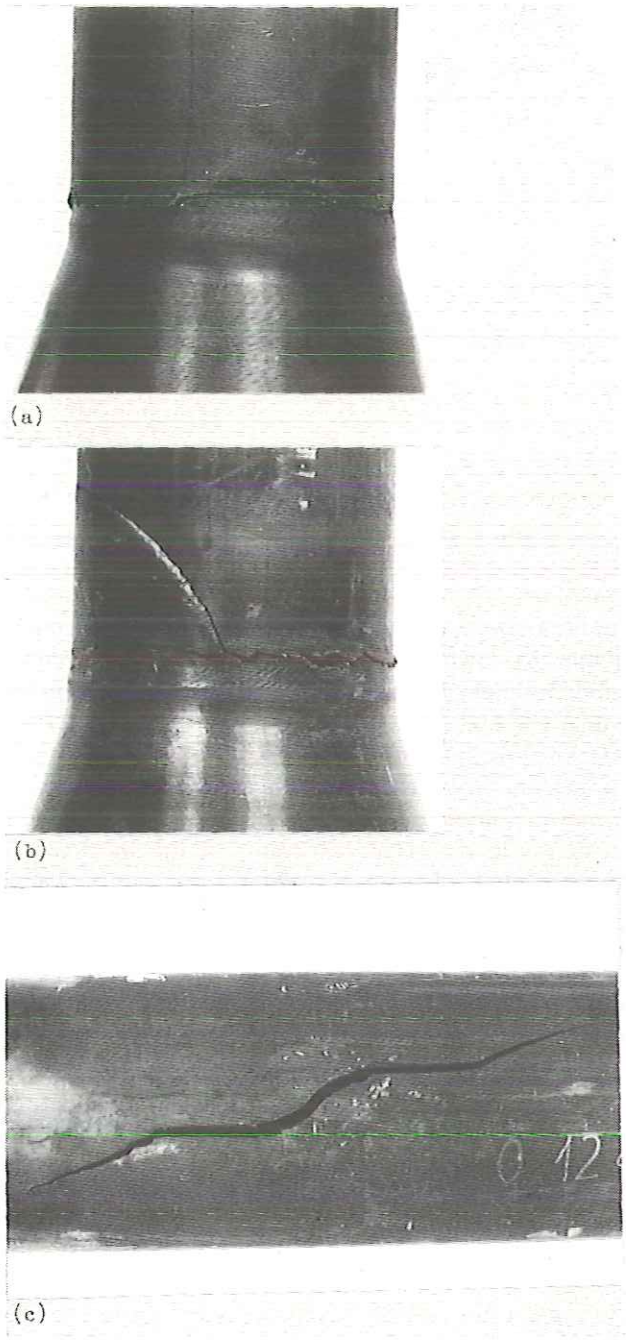

Fig 7 Typical aspects of fatigue ruptures for (a) $R = 1$, (b) $R = 3.4$, and (c) $R = \infty$

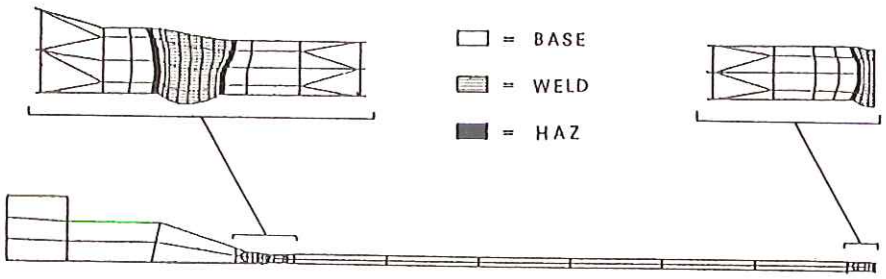

Fig 8 Finite element idealization of multiaxial specimens

inelastic analysis of the tubular specimen was performed by means of the non-linear INCA (9) finite element code.

The axially symmetric idealisation of one half of the specimen is shown in Fig. 8. For each of the various metallurgical structures which prevail in the various zones of the specimen the appropriate cyclic stress–strain response was assumed with reference to equation (1).

Since the real weld geometry varied from point to point, for each weldment both the 'worst' and the 'best' shape observed on the real specimens were modelled.

The calculations were repeated for the various uniaxial and multiaxial loadings used in the tests by imposing the experimental values of axial and/or angular displacements to the flanged end. General agreement was checked for each run between the nominal test strain and those calculated in the elements sufficiently far from the notch zones. As can be observed in Fig. 9 the use of the

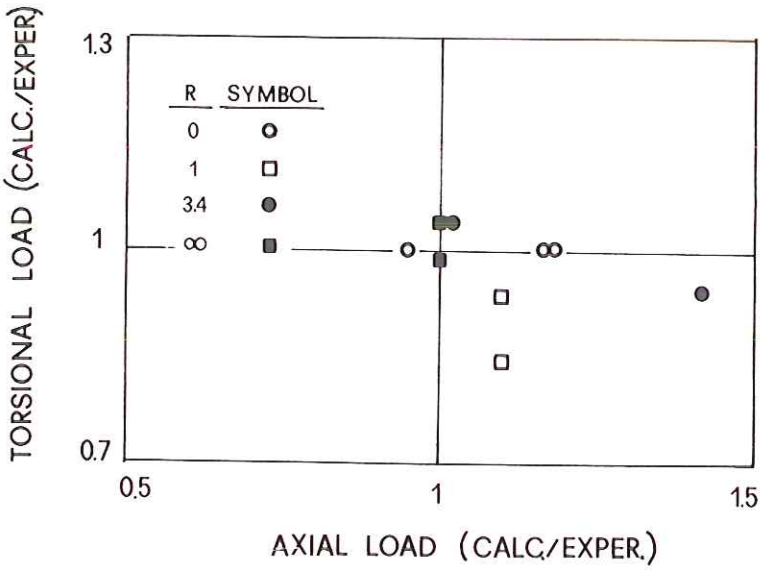

Fig 9 Ratios of calculated and experimental loads: torsional vs axial ratios

cyclic stress–strain curves also provided an acceptable agreement between calculated axial and torsional loads and experimental values measured at half life in each test.

Some additional calculations, performed assuming constant material properties across the weld (i.e., base material properties everywhere), underestimated the maximum local strain, which, in the present case, is significantly influenced by the 'metallurgical notch effect' (**10**).

Discussion

Experimental rupture data were compared with life predictions based on various methodologies. At first the ASME design rules for elastic analysis (**3**) were applied. They are based on the nominal equivalent von Mises strain range and on the evaluation of the strain concentration effects by means of a simplified application of Neuber's rule.

Theoretical stress concentration factors (K_t) in the weldments, required for this kind of analysis, were evaluated by elastic finite element calculations, and were found to vary between 1.26 and 1.55 in axial loading, and between 1.07 and 1.11 in pure torsional loading.

When applying the above-indicated criterion in multiaxial strain conditions two methods are allowed by the ASME rules.

According to the first method, first the nominal equivalent strain range is evaluated, then the maximum local value of the equivalent strain is obtained for each strain state, using the highest value of K_t in any loading direction.

By the second method a somewhat more accurate analysis is performed, since different stress concentration factors are used for the individual strain components. In the present case this corresponds to the assumption of the above-indicated values of K_t for the axial and torsional components of the nominal strain. The maximum equivalent strain is then calculated from the local values of the axial and torsional components.

With reference to the inelastic analysis ASME rules, another methodology was used, based on the evaluation of local elasto–plastic strain ranges in the weldments by means of the finite element method. The results of the calculations must be interpreted, to evaluate significant strain range values in the most stressed zones. These latter coincide with the weld toes in the central and end weldments (see Fig. 8).

In the following application, the maximum value of the computed equivalent strains in the finite elements near the weld toe (whose side is about 0.6 mm long) was taken as a significant parameter to evaluate the strain history of the most-stressed volumes of material, where a crack may nucleate owing to low cycle fatigue phenomena.

For each of the above indicated methods the life was then predicted with reference to the fatigue resistance relationship (equation 2).

Finally, stress and strain component data calculated by the finite element

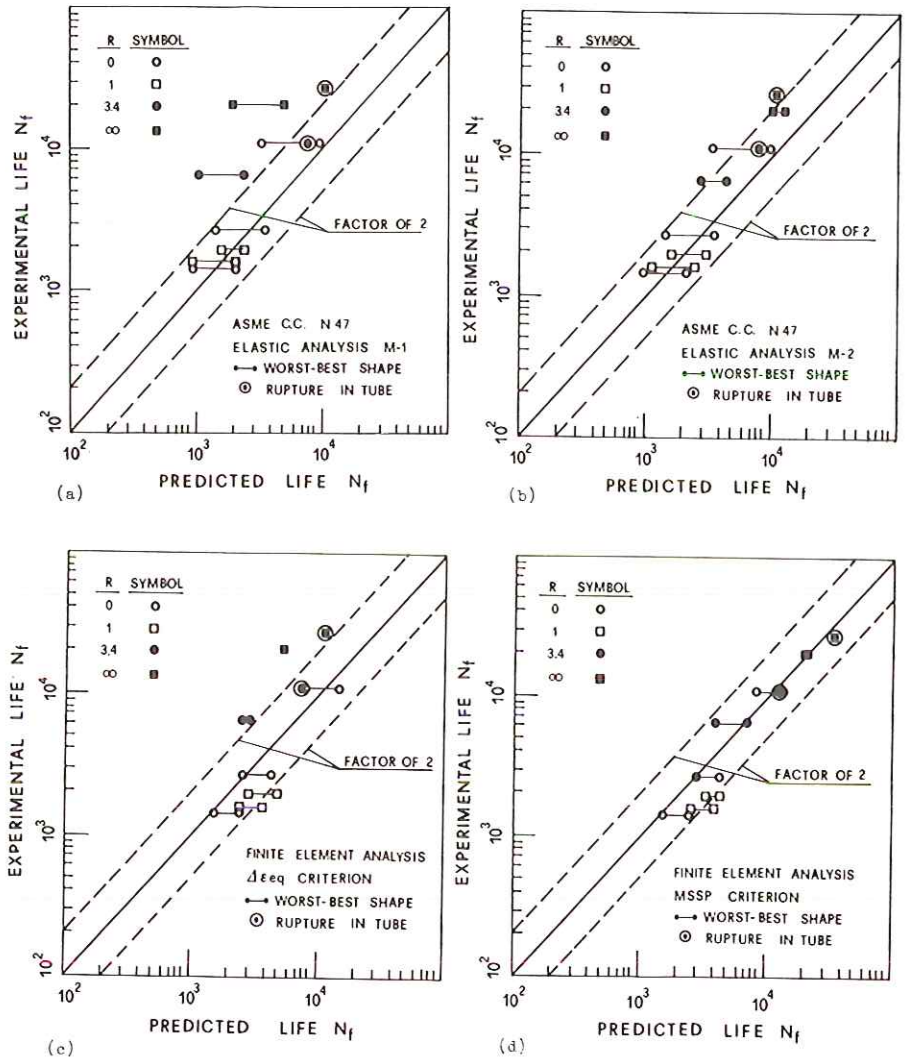

Fig 10 Experimental life vs cycles at rupture predicted by 'elastic analysis' with (a) method 1, (b) method 2, (c) FE inelastic analysis with equivalent strain, and (d) MSSP criterion

analysis were introduced in a post-processing program in order to evaluate the normal and shear strains on the maximum shear stress plane (MSSP) (**11**).

The evaluation of the predicted number of cycles at failure was then performed following the Brown and Miller method by interpolating the multiaxial fatigue resistance curves reported in (**6**).

The results of the application of the various methods described are illustrated in Fig. 10 and summarized in Table 4.

Table 4 Predicted rupture lives (best–worst shapes)

	Elastic analysis		*Inelastic analysis (FEM)*	
Test No.	*Method 1*	*Method 2*	*Equivalent strain*	*MSSP*
108	2109–960	2109–960	2437–1543	2550–1600
102	3639–1481	3639–1481	4519–2572	4500–3000
104	9648–3358	9648–3358	15 179–7970	14 000–8200
125	2521–1649	3101–1649	4829–2978	4500–3400
143	2094–954	2469–1169	3860–2486	4000–2700
126	7813	7813	7618	12 733
145	2456–1081	4377–2826	2950–2572	6936–4000
124	10 858	10 858	11 197	34 000
144	5317–2055	12 983–10 085	5567	21 300

It appears that the life predictions performed by the elastic analysis ASME rules (methods No. 1 and No. 2) are both conservative. The results obtained with the larger torsional strains are the most conservatively predicted and the simpler method No. 1 (Fig. 10(a)) is more conservative than the other, whose predictions approximate the ± 2 factor scatterband (Fig. 10(b)).

The inelastic analysis results, used in accordance with ASME rules (equivalent von Mises strain) give rise to less scattered predictions, but the same above-indicated trend can still be observed (Fig. 10(c)), while the predictions are, on the whole, less conservative.

The best correlation between prediction and experimental values is obtained by the Brown and Miller approach (MSSP method).

Conclusions

A simple welded structural element subjected to multiaxial low cycle fatigue at high temperature was analysed with the aim of comparing life predictions obtained by several particular methods and experimental results.

Experimentally it was observed that, for the same equivalent strain range, the low cycle fatigue life is longer when the nominal strain-state (multiaxiality) ratio is greater. It was appreciated that the strain pattern, as evaluated for various strain-state ratios by a non-linear finite element code, is significantly influenced by the different cyclic stress–strain behaviour of the materials of the various zones of the weldments.

The simplest of the elastic analysis design methods, based on the evaluation of the maximum theoretical stress concentration factor, on Neuber's rule, and on the von Mises' equivalent strain, gave conservative life predictions.

If an inelastic analysis is performed, its results are better interpreted by the application of the Brown and Miller method, the life predictions of which are much less influenced by the multiaxiality of the state of strain. However, the Brown and Miller approach requires the knowledge of fatigue data obtained by multiaxial tests and is not particularly straightforward in the evaluation of the

MSSPs and the most critical zones. Post-processing of the inelastic analysis results would, therefore, be necessary in real applications.

Acknowledgements

The authors wish to thank Dr Enrico Ciulli and Mr Sergio Martini of the University of Pisa for helpful cooperation regarding the computer code applications and the uniaxial and multiaxial experiments. This research was supported by the Italian National Committee for Nuclear Energy (ENEA).

References

(1) BROWN, H. W. and MILLER, K. J. (1978) High temperature biaxial fatigue of two steels. *Fatigue Engng Mater. Structures*, **1**, 217–229.
(2) BROWN, M. W. and MILLER, K. J. (1979) Initiation and growth of cracks in biaxial fatigue. *Fatigue Engng Mater. Structures*, **1**, 231–246.
(3) *Class 1 components in elevated temperature service*, Sect. III, Div. 1, Case N47-24 of the ASME Boiler and Pressure Vessel Code (1984), ASME, New York.
(4) VITALE, E. and TESI, B. (1984) Indagine, mediante una tecnica di simulazione, sulle proprieta' meccaniche della ZTA in giunti saldati di AISI 316. *Rivista Italiana della Saldatura*, **3**, 1–7.
(5) VITALE, E. (1984) Characterization of the stress–strain behaviour in type 316 welded joints. *Proceedings of the International Conference on Creep and Fracture of Engineering Materials and Structures*, Pineridge Press, Swansea, pp. 851–859.
(6) KANDIL, F. A., BROWN, M. W., and MILLER, K. J. (1982) Biaxial low cycle fatigue failure of 316 stainless steel at elevated temperature. *Proceedings of the International Conference on Mechanical Behaviour and Nuclear Applications of Stainless Steels at Elevated Temperatures*, Metals Society (Book 280), London.
(7) MANFREDI, E., VITALE, E., and BERTINI, L. (1982) Austenitic stainless steels type AISI 304 and 316 under cyclic loads. University of Pisa, Dept. Mechanical and Nuclear Engineering DCMN004(82), Pisa.
(8) DEL PUGLIA, A., MANFREDI, E., and VITALE, E. (1982) Creep fatigue in AISI stainless steel welded structures. *Proceedings of the International Conference on Mechanical Behaviour and Nuclear Applications of Stainless Steel at Elevated Temperature*, Metals Society (Book 280), London.
(9) *Manuel de INCA* (1983), CISI Compagnie Internationale de Services en Informatique, Paris.
(10) VITALE, E. and JERACITANO, G. (1983) Analisi del comportamento di modelli strutturali e di provini in AISI 316 soggetti a fatica ad elevata temperatura. University of Pisa, Dept. of Mechanical and Nuclear Engineering RL041(83), Pisa.
(11) KANAZAWA, K., BROWN, M. W., and MILLER, K. J. (1977) Low cycle fatigue under out of phase loading conditions. *Trans ASME, J. Engng Mater. Technol.*, July, 222–228.